RSC Advances

ROYAL SOCIETY OF CHEMISTRY

www.rsc.org/advances

TABLE OF CONTENTS ENTRY

Synthesis and Self-assembly Behavior of Organic-inorganic Macrocyclic Molecular Brushes Composed of Macrocyclic Oligomeric Silsesquioxane and Poly(N-isopropylacrylamide)

Yulin Yi and Sixun Zheng *

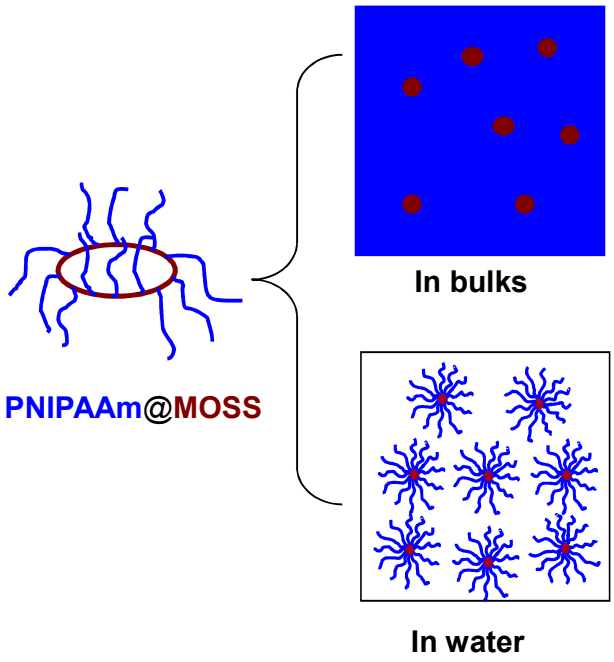

Macrocyclic molecular brushes composed of macrocyclic oligomeric silsesquioxanes and poly(N-isopropylacrylamide) were synthesized *via* ATRP approach; they displayed the self-assembly behavior.

Synthesis and Self-assembly Behavior of Organic-inorganic Macrocyclic Molecular Brushes Composed of Macrocyclic Oligomeric Silsesquioxane and Poly(N-isopropylacrylamide)

Yulin Yi and Sixun Zheng*

Department of Polymer Science and Engineering and the State Key Laboratory of Metal Matrix Composites, Shanghai Jiao Tong University, Shanghai 200240, China

* To whom correspondence should be addressed. Tel: 86-21-54743278; Fax: 86-21-54741297; Email: *szheng@sjtu.edu.cn* (*S. Zheng*).

ABSTRACT

The novel organic-inorganic molecular brush composed of macrocyclic oligomeric silsesquioxane (MOSS) and poly(N-isopropyl acrylamide) (PNIPAAm) (denoted PNIPAAm@MOSS) was synthesized *via* the atom transfer radical polymerization (ATRP) approach. In bulks, the organic-inorganic molecular brushes were microphase-separated; the spherical MOSS microdomains with the size of 10 ~ 50 nm in diameter were dispersed into continuous PNIPAAm matrix. Depending on the lengths of PNIPAAm chains, the PNIPAAm@MOSS molecular brushes were capable of self-assembling into the cylindrical or spherical nanoobjects in aqueous solutions as evidenced by transmission election microscopy (TEM) and dynamic light scattering (DLS). Both micro-differential scanning calorimetry (Micro-DSC) and ultraviolet-visible spectroscopy showed that the MOSS backbones exerted significant restriction of coil-to-globule transition of PNIPAAm chains.

(**Keywords:** macrocyclic oligomeric silsesquioxane; poly(N-isopropylacrylamide); macrocyclic molecular brushes; thermoresponse; self-assembly)

INTRODUCTION

Responsive or "smart" materials have attracted considerable interest owing to their promising potential applications in biomedical fields [1-6]. Poly(N-isopropylacrylamide) (PNIPAAm) is among the mostly investigated thermoresponsive polymers. In aqueous solutions, PNIPAAm can display a lower critical solution temperature (LCST) at about 32 °C [7-11]. Below this temperature, individual PNIPAAm chains adopt a random coil conformation and the random coils would collapse into globules upon heating the aqueous solutions up to *c.a.* 32 ^{o}C, *i.e,* so-called coil-to-globule transition occurs. It is realized that there are the intermolecular hydrogen bonding interactions between amide groups of PNIPAAm and water molecular at lower temperatures, which promote the water-solubility of this polymer. Upon heating the solution up to 32 ^{o}C or above, the intermolecular hydrogen bonding interactions are interrupted owing to the conformational changes of PNIPAAm chains. In the past decades, the thermoresponsive behavior of PNIPAAm has been extensively investigated. It has been known that some structural factors such as co-monomer, tacticity, crosslinking, grafting, molecular weights and end groups all affect the LCST behavior of PNIPAAm in aqueous solutions [12-18].

Recently, considerable attention has been paid to the preparation of PNIPAAm amphiphiles containing hydrophobic structural units since these PNIPAAm-containing amphiphiles are capable of self-assembling into a variety of thermoresponsive nanoobjects in aqueous solutions. The self-assembly behavior of the PNIPAAm amphiphiles can exert a profound influence on the thermoresponsive behaviors of this polymer [8,19,20]. For instance, Winnik *et al.* investigated the effect of the hydrophobic *n*-octadecyl termini on the merging of mesoglobules of PNIPAAm and proposed that the rigidity and partial vitrification of mesoglobules may be the prevalent cause of their stability against aggregations [8]. Zhang *et al* [21] investigated the self-assembly of PS-*b*-PNIPAAm-*b*-PS triblock copolymers in aqueous solutions and reported the formation of flower-like aggregates with PNIPAAm interlocking rings and associating PS blocks as the core and PNIPAM rings as the coronas. It was found that the morphologies of micelle-like aggregates can significantly affect the collapse transition of PNIPAAm coronas. More recently, the PNIPAAm amphiphiles containing bulky and hydrophobic inorganic groups attract considerable interest owing to the specific architectures and self-assembly

behavior of this class of organic-inorganic hybrids [22-28]. Polyhedral oligomeric silsesquioxane (POSS)-capped semi-telechelic PNIPAAm hybrids have been synthesized *via* reversible addition-fragmentation chain transfer (RAFT) or atom transfer radical polymerization (ATRP) [24,25] and these organic-inorganic PNIPAAm amphiphiles can be self-assembled into the thermoresponsive nanoobjects. Wang *et al.* [26] reported synthesis of α,ω-diPOSS-capped PNIPAAm telechelics with a "POSS-spreading" strategy. In this approach, a diPOSS-bearing trithiocarbonate was synthesized and used as a chain transfer agent, with which the RAFT polymerization of NIPAAm was carried out and two ends of PNIPAAm chain were capped with hepta(3,3,3-trifluropropyl) POSS. Owing to the high hydrophobicity of the POSS end groups, these POSS-capped PNIPAAm telechelics can form organic-inorganic physical hydrogels in water. These physical hydrogels displayed fast deswelling and reswelling properties compared to traditional chemically crosslinked hydrogels. Kuo *et al* [27] reported the synthesis of octa-armed PNIPAAm stars with POSS cores. It was found that these organic-inorganic PNIPAAm stars undergo a sharp coil-to-globule transition in water at about 32 ^{o}C, which is similar to linear PNIPAAm homopolymers. More recently, He *et al* [28] investigated the thermoresponsive and pH dual-responsive behaviors of a star-like block copolymers with POSS core and poly(N-isopropylacrylamide)-*block*-poly(acrylic acid) diblock copolymer arms. The results showed that with the star-block architecture, the high local chain density near POSS core may lead to enhanced intramolecular interactions between different types of units and hence significantly alter the critical phase transition behavior.

Polyhedral oligoalkylmetallasiloxanes are a class of novel organometallic compounds, which consist of stereoregular alkylsiloxane macrocycles coordinated to alkaline and/or transition metals (*e.g,* Mn, Co, Ni, Cu and trivalent lanthanide metals) [29-37]. These metallasiloxane coordinates can conveniently be converted into macrocyclic oligomeric silsesquioxanes (MOSS) with satisfactory yields, which are potential to be used as a new family of building blocks for organic-inorganic hybrids [38-41]. In this work, we explored the synthesis of the organic-inorganic macrocyclic molecular brushes composed of MOSS backbone and PNIPAAm arms. Toward this end, we firstly synthesized a twenty-four-membered MOSS macromer bearing twelve 2-chloropropionate moieties and then functionalized MOSS was used as a macroinitiator for the atom transfer radical polymerization of N-isopropylacrylamide

(NIPAAm) to afford the organic-inorganic macrocyclic molecular brushes. The purpose of this work is twofold: i) to explore the synthesis of the organic-inorganic macrocyclic molecular brushes with a inorganic macrocyclic molecule as the backbone and PNIPAAm as side chains and ii) to investigate the effect of the organic-inorganic macrocyclic brush architectures on the thermoresponsive and self-assembly behavior of PNIPAAm. In the past years, the thermoresponsive and self-assembly behavior of a variety PNIPAAm amphiphiles has been extensively investigated. To the best of our knowledge, nonetheless, there has been no previous report on the studies on the organic-inorganic PNIPAAm macrocyclic brushes. In this work, the thermoresponsive and self-assembly behavior of the organic-inorganic macrocyclic molecular brushes were addressed on the basis of the results of transmission electronic microscopy (TEM), micro-differential scanning calorimetry (Micro-DSC), UV-vis spectroscopy and dynamic laser scattering (DLS).

EXPERIMENTAL

Materials

Organic silanes (*i.e,* methyltriethoxysilane and dimethylchlorosilane) were purchased from Gelest Co, USA and used as received. Copper (II) chloride ($CuCl_2$) was obtained from Ruanshi Chemical Co, Jiangsu, China. Sodium hydroxide (NaOH), silver nitrate ($AgNO_3$), pyridine and organic solvents such as anhydrous ethanol, methanol and toluene were purchased from Shanghai Reagent Co, Shanghai, China. Before use, toluene and pyridine were distilled over calcium hydride (CaH_2) and then stored in a sealed vessel in the presence of 4Å molecular sieve. N-isopropylacrylamide (NIPAAm) was prepared in this lab *via* the reaction between isopropylamine and acryloyl chloride. Copper (I) chloride (CuCl) was of chemically pure grade, supplied by Shanghai Reagent Co. China. Tris(2-(dimethylamino)ethyl)amine (Me_6TREN) was prepared by following the methods reported by Matyjaszewski *et al.* [42]. All other solvents used were obtained from commercial sources. Before use, tetrahydrofuran (THF) was refluxed above sodium and distilled; triethylamine (TEA) and isopropyl alcohol (IPA) were dried over CaH_2 and then distilled; N,N-dimethylformamide (DMF) was dried over anhydrous magnesium sulfate and distilled under reduced pressure.

Synthesis of Dodecamethyldodeca(dimethylhydro)cyclododecasilsesquioxane (1)

First, the coordinate of the metals (*i.e,* alkaline and copper) with methylsiloxanolates was prepared *via* the reactions between methyltriethoxysilane[$MeSi(OEt)_3$] and copper (II) chloride ($CuCl_2$) in the basic media (*e.g,* NaOH) by following the methods of literature reported by Shchegolikhina *et al.* [43,44]. Second, the coordinate (8.480g, 4.99mol) was added to the mixture composed of anhydrous toluene (160 mL), dimethylchlorosilane [$(CH_3)_2SiHCl$)] (42.000g, 442.1 mmol) and pyridine (28.400g, 359.1mmol) at room temperature. The reaction was carried out at 25 ^oC for 24 hours with vigorous stirring. The mixture was filtered to isolate the precipitates and the solution was washed with deionized water until no chlorine ions were detected with aqueous solution of silver nitrate ($AgNO_3$). After dried with anhydrous $MgSO_4$, all the solvents were eliminated with rotary evaporation to afford 7.36 g viscous liquid (*i.e,* compound **1**) with the yield of 98.0 %. ^1H NMR ($CDCl_3$): 4.72 (*m,* 1H, Si**H**), 0.205- 0.194 [*d*, 6H, $Si(C\mathbf{H}_3)_2$], 0.10 (*s*, 3H, $O_3SiC\mathbf{H}_3$). ^{29}Si NMR (ppm, $CDCl_3$): -66.2 (*d*, **Si**$O_{3/2}$), -6.4 [*s*, **Si**$(CH_3)_2H$].

Synthesis of Allyl 2-chloropropionate (2)

To a flask equipped with a magnetic stirrer, dichloromethane (80 mL), triethylamine (18.200g, 180mmol) and allyl alcohol (8.350g, 144mmol) were charged with vigorous stirring and then 2-chloropropionyl chloride (18.0g, 141.7mmol) was added at 0 ^oC. The reaction was performed at 0^oC for 2 hours and at room temperature for 24 hours. The mixture was washed with deionized water and the solvent was eliminated *via* rotary evaporation. The product (19.400g) was obtained *via* distillation at reduced pressure with the yield of 92.1%. ^1H NMR (ppm, $CDCl_3$): 5.96-5.87 (*m,* 1H, CH_2=C**H**$CH_2OOCCHClCH_3$), 5.38-5.26 (*m,* 2H, C$\mathbf{H_2}$=$CHCH_2OOCCHClCH_3$), 4.68-4.66 (*m,* 2H, CH_2=$CHC\mathbf{H}_2OOCCHClCH_3$), 4.45-4.39 (*q,* 1H, CH_2=$CHCH_2OOCC\mathbf{H}ClCH_3$), 1.71-1.69 (*d,* 3H, CH_2=$CHCH_2OOCCHClC\mathbf{H_3}$).

Synthesis of MOSS Macromolecular Initiator (3)

To a flask equipped with a dried magnetic stirrer, anhydrous toluene (24 mL), compound **1** [*i.e.*, dodecamethyldodeca(dimethylhydro)cyclododecasilsesquioxane)]

(2.400g, 1.492mmol) and compound **2** (*viz.* allyl 2-chloropropionate) (4.000g, 26.88 mmol) were charged with vigorous stirring. The flask was connected onto a Schlenk line to degas *via* three freeze-pump-thaw cycles and Karstedt catalyst (80 μL) was added with a syringe. The reaction was carried out at 85 ^{o}C for 10 hours. The solvent and unreacted allyl 2-chloropropionate was eliminated *via* rotary evaporation and the product (4.600g) (*i.e.,* compound **3**) was obtained with the yield of 92.0%. ^{1}H NMR (ppm, $CDCl_3$): 4.42-4.30 (*q*, 1H, C**H**Cl), 4.16-4.06 (*s*, 2H, COOC**H**$_2$), 1.75-1.61 (*d*, 5H, ClCHC**H**$_3$, C**H**$_2$CH$_2$Si), 0.63-0.54 [*t*, 2H, CH$_2$C**H**$_2$Si], 0.20-0.03 [*t*, 9H, O$_3$SiC**H**$_3$, O$_2$Si(C**H**$_3$)$_2$]. ^{29}Si NMR (ppm, $CDCl_3$): -66.2 (*d*, **Si**O$_{3/2}$), -6.4 [*s*, **Si**(CH$_3$)$_2$CH$_2$CH$_2$CH$_2$OOCCHClCH$_3$].

Synthesis of Organic-Inorganic Molecular Brushes

Typically, to a flask equipped with a magnetic stirrer, the above MOSS macromolecular initiator (*i.e.,* compound **3**) (0.18g, 0.64mmol with respect of allyl 2-chloropropionate group), NIPAAm (2.70g, 23.8 mmol) and isopropyl alcohol (6 mL) were charged with vigorous stirring. The flask was connected onto the Schlenk line to degas *via* three freeze-pump-thaw cycles and then copper (I) chloride (29.60 mg), Me_6Tren (87 μL) were added. The system was purged with highly pure nitrogen for 45 min and the polymerization was performed at room temperature for 24 hours. After that, 20 mL of tetrahydrofuran was added to dissolve the reacted product and the solution was passed through a neutral alumina column to remove the catalyst. The solution was concentrated *via* rotary evaporation and then dropped into 200 mL of petroleum ether to afford the precipitates. The precipitates were re-dissolved in tetrahydrofuran and the as-obtained solution was re-dropped into petroleum ether to obtain the precipitates. After dried *in vacuo* at 30 ^{o}C for 24 hours, the polymer (2.1g) was obtained with the conversion of PNIPAAm to be 71%. ^{1}H NMR (400MHz, $CDCl_3$): 6.06-6.57 [*m,* -N**H**CH(CH$_3$)$_2$], 4.02 [*s*, NHC**H**(CH$_3$)$_2$], 2.4-1.2 [*m*, C**H**$_2$C**H**], 1.14 (*d*, CH(C**H**$_3$)$_2$), 0.02-0.18 [*m*, O$_3$SiC**H**$_3$ and O$_2$Si(C**H**$_3$)$_2$]. GPC: M_n=36,200 with M_w/M_n=1.46.

Measurement and Techniques

Nuclear Magnetic Resonance Spectroscopy (NMR)

The ^{1}H NMR measurement was carried out on a Varian Mercury Plus 400 MHz NMR spectrometer at 25 ^{o}C and the ^{29}Si NMR spectra were obtained on a Bruker Avance III 400 MHz NMR spectrometer. The samples were dissolved with deuterated chloroform ($CDCl_3$) and the solutions were measured with tetramethylsilane (TMS) as an internal reference.

Matrix-Assisted Ultraviolet Laser Desorption / Ionization Time-of-Flight Mass Spectroscopy (MALDI-TOF-MS)

Gentisic acid (2,5-dihydroxybenzoic acid, DHB) was used as the matrix with dichloromethane as the solvent. The MALDI-TOF-MS experiment was carried out on an IonSpec HiResMALDI mass spectrometer equipped with a pulsed nitrogen laser (λ = 337 nm; pulse with = 3 ns). This instrument operated at an accelerating potential of 20 kV in reflector mode. Sodium is used as the cationizing agent and all the data shown are for positive ions.

Gel Permeation Chromatography (GPC)

The molecular weights and molecular weight distribution of polymers were determined on a Waters 717 Plus autosampler gel permeation chromatography apparatus equipped with Waters RH columns and a Dawn Eos (Wyatt Technology) multiangle laser light scattering detector and the measurements were carried out at 25 ^{o}C with dimethylformamide (DMF) as the eluent at the rate of 1.0 mL/min.

Micro-Differential Scanning Calorimetry (Micro-DSC)

The Micro-DSC measurements were performed with a SETARAM micro-DSC III system under dry nitrogen atmosphere and circulating water. Before the measurement, the specimens were maintained at 18 ^{o}C for 15 min and were then heated to 60 ^{o}C at the heating rate of 1 ^{o}C/min. The temperature at the minimum of exothermic peak was taken as the lower critical solution temperature (LCST).

Determination of Cloud Point

Each polymer (0.01 g) was dissolved in the 0.5 mL of tetrahydrofuran (THF) and then the solution was dropwise added into 50 mL of ultrapure water by a dropping funnel with vigorous stirring. After that, the suspension was stirred for additional 30 min and a transparent emulsion was formed with the concentration of the polymer being 0.2 g/L. The solvent (*i.e,* THF) in the suspension was eliminated *via* rotary evaporation for 2 hours. The cloud points were determined with an Agilent Technologies Cary 60 Ultraviolet-visible spectrometer at the wavelength of light to be λ=550 nm. In the measurements, a thermostatically controlled cuvette holder was employed and the plots of light transmittance as a function of temperature were obtained.

Dynamic Laser Scattering (DLS)

The above suspensions of PNIPAAm@MOSS at the concentration of 0.2 g/L were subjected to dynamic laser scattering (DLS). The laser light scattering experiments were conducted on a Malvern Nano ZS90 equipped with a He-Ne laser operated at the wavelength of λ = 633 nm and the data were collected at a fixed scattering angle of 90^{o}.

Transmission Electron Microscopy (TEM)

The morphological observations were conducted on a JEOL JEM 2100F electron microscope at a voltage of 200 kV. To investigate the morphology of the samples in bulks, the THF solutions of the polymers at the concentration of 1 wt% were cast on carbon-coated copper grids and the solvent was slowly evaporated at room temperature and then *in vacuo* at 30 ^{o}C for 2 hours. The specimens were directly observed without an additional staining step. To investigate the self-assembly behavior of the samples in aqueous solutions, the specimens were prepared by dropping the suspensions of the polymer in water (about 10 μl at 0.2 g × L^{-1}) onto carbon-coated copper grids; the water was eliminated *via* freeze-drying approach.

RESULTS AND DISCUSSION

Synthesis of Organic-inorganic Molecular Brushes

The route of synthesis for the organic-inorganic macromolecular brushes composed of macrocyclic oligomeric silsesquioxane (MOSS) and poly(N-isopropyl acrylamide) (PNIPAAm) (denoted PNIPAAm@MOSS) is shown in Scheme 1. Firstly, the MOSS macromolecular initiator bearing 2-chloropropionate moieties was synthesized *via* the hydrosilylation reactions of dodecamethyldodeca (dimethylhydro)cyclododecasilsesquioxane (compound **1**) with allyl 2-chloropropionate (compound **2**). Compound **1** was synthesized *via* the silylation reaction of the coordinate of copper and sodium with methysiloxanolate (*i.e,* nickel/sodium dodecamethyldodecasiloxanolate□) with dimethylchlorosilane. The metallasilsesquioxanes used in this work was prepared *via* the reaction of methyltriethoxylsiloxane [$CH_3Si(OCH_2CH)_3$] with sodium hydroxide (NaOH) and copper (II) chloride ($CuCl_2$) in the presence of water and alcohol by following the method of literature reported by Sergienko *et al.* [43,44]. It was reported that the crystal of the coordinate possessed a globular structure, in which the twelve-$SiO_{3/2}$-membered organosiloxanolate ligand [*i.e,* $vinylSi(O)O^{-1}]_{12}$ in the tris-*cis*-tris-*trans* configuration constituted a saddle conformation, which was fixed by four Cu(II) ions. The metallacyclosiloxanolate was allowed to react with the dimethylchlorosilane to afford the macrocyclic oligomeric silsesquioxane bearing twelve Si-H bonds (compound **3**). The ^{29}Si NMR spectrum of compound **3** is shown in Figures 1. In the ^{29}Si NMR spectrum, two resonance peaks were detected at -6.4 and -66.2 ppm, respectively. The former is assignable to the silicon nucleus bonded with hydrogen atom (*i.e.,* that in Si-H bond) whereas the latter to the nucleus of silicon of macrocyclic backbones. The appearance of the two resonance peaks indicates that the compound had a macrocyclic structures with silsesquioxane as the backbone and with hydrodimethylsiloxyl as side groups. It should be pointed out that the baseline uplifting of the spectral line in the range of -75 to -100 ppm resulted from the resonance of ^{29}Si nucleus in the NMR tube. The expanded ^{29}Si NMR spectrum shows that the signal of resonance at -66.15 ppm was composed of two splitting peaks to have very close chemical shifts and the ratio of integral intensity of the peak at -66.11 ppm to -66.37 ppm was 2:1. The splitting of silicon resonance signal was related to the configuration of the MOSS macromer. It is proposed that

trimethylsiloxyl groups appeared in the 24-membered macrocyclic silsesquioxane with the tris-*cis*-tris-*trans* configuration. Compound **3** was subjected to MALDI-TOF mass spectroscopy to measure its molecular weight and its mass spectrum was shown in Figure 2. A group of intense peaks centered at the value of M/Z to be 1633.3 were detected, implying that the compound possessed the molecular weight of 1610 Da. The molecular weight is exactly identical with the value estimated according to the formula of compound **3.** The ^{29}Si NMR and MALD-TOF mass spectroscopy indicates that the MOSS macromer bearing twelve Si-H bonds was successfully obtained.

The hydrosilylation reaction of the MOSS macromer (*viz.* compound **3**) with allyl 2-chloropropionate (**2**) was carried out to afford dodecamethyldodeca(dimethylpropyl-2-chloropropionate)cyclododecasilsesquioxane (compound **4**), *i.e.,* a MOSS macromolecular initiator bearing 2-chloropropionate moieties. Also shown in Figure 1 is the ^{29}Si NMR spectrum of compound 4. Compared to the ^{29}Si NMR spectrum of compound **1**, the positions of the resonance peaks assignable to the silicon nucleus of MOSS backbone (at -66.2 ppm) and the side groups (at -6.4 ppm) remained almost invariant, indicating that the hydrosilylation reaction did not alter the structures of macrocyclic silsesquioxane. Shown in Figure 3 are the ^{1}H NMR spectra of compounds **3** and **4**. For compound **3**, the resonance peaks of methyl and Si-H protons were detected at 0.09, 0.203 and 4.73 ppm, respectively. The former two peaks are assignable to the protons of methyl groups connected to silsesquioxane backbone and the methyl in dimethylhydrosiloxayl groups, respectively. The resonance at 4.73 ppm is attributable to the protons in Si-H bonds. The ratio of integral intensity for these protons was measured to be 3 : 6 : 1, which is in good agreement with the value calculated according to the structural formula of compound **3**. Compared to the ^{1}H NMR spectrum of compound **3**, the signal of resonance at 4.73 ppm assignable to the protons of Si-H bonds completely disappeared, suggesting that the hydrosilylation has been performed to completion. Concurrently, there appeared several new signals of resonance at 0.57, 1.69, 2.45, 1.98, 4.11 and 4.38 ppm, which are assignable to the protons of propyl 2-chloropropionate moiety as indicated in this figure. The ^{1}H and ^{29}Si NMR spectroscopy indicates that the MOSS macromer bearing 2-chloropropionate moiety was successfully obtained.

The MOSS macromer bearing 2-chloropropionate moieties was used as the macromolecular initiator and the atom transfer radical polymerization (ATRP) was

carried out to afford the organic-inorganic macromolecular brushes with MOSS backbone and with poly(N-isopropyl acrylamide) (PNIPAAm) arms (See Scheme 1). By controlling the molar ratio of the macromolecular initiator to NIPAAm and the conversion of the monomer, the organic-inorganic molecular brushes with variable lengths of PNIPAAm were obtained. Representatively shown in Figure 3 is the ^{1}H NMR spectrum of PNIPAAm2K@MOSS. The signals of resonance at 1.14, 1.64, 2.02 and 4.01 ppm are assigned to the proton resonance of methyl, methylene, methine of PNIPAAm main chain, methine of isopropyl groups of PNIPAAm, respectively; the broad signals of resonance at 6.0 ~ 7.0 ppm were assignable to the protons of N-H moiety. The signal of proton resonance at 0.10 ppm was discernable and is assignable to the protons of methyl groups of MOSS backbone. The ^{1}H NMR spectroscopy indicates that this product combined the structural features from PNIPAAm and MOSS. All the PNIPAAm@MOSS samples with variable lengths of PNIPAAm chains together with compound **4** were subjected to gel permeation chromatography (GPC) to measure the molecular weights and the GPC profiles are presented in Figure 4. The results of the molecular weights are summarized in Table 1. In all the cases the unimodal peaks were displayed and no MOSS macromolecular initiator was detected in the resulting samples. Shown in Figure 5 are the plots of number-average molecular weights and the values of polydispersity index as functions of the molar ratio of NIPAAm to the MOSS macromolecular initiator. It is seen that the molecular weights almost linearly increased with increasing the molar ratio of NIPAAm to the MOSS macromolecular initiator; the polydispersity indices of the PNIPAAm@MOSS were in the range of 1.30~1.46. The unimodal and fairly narrow distribution of molecular weights indicates that the MOSS macroinitiator (compound **4**) can be used to obtain the PNIPAAm@MOSS samples, *i.e,* the organic-inorganic molecular brushes were successfully obtained and that the the polymerizations of NIPAAm with the MOSS macromolecular imitator were in a living and controlled manner. It is noted that while the PNIPAAm arms were short (*e.g.*, PNIPAAm2K@MOSS and PNIPAAm4K@MOSS) the distribution of the molecular weights were relatively broad. This observation could be accounted for the restriction of the MOSS macrocycle on the ATRP of NIPAAm. In this work, the lengths of PNIPAAm arms were also estimated by means of thermogravimetric analysis (TGA). Assuming that the ceramic residues of the degradation were from MOSS, the lengths of PNIPAAm arms were thus estimated according to the in the yields of degradation (the TGA

curves not shown for brevity) and the results were also incorporated into Table 1. It is seen that the values of molecular weights by GPC were lower than those estimated by TGA. This observation could be ascribed to the relatively low hydrodynamic volumes of the brush-like PNIPAAm samples.

LCST Behavior

It is known that PNIPAAm chains are capable of undergoing a coil-to-globule transition in aqueous solution in the vicinity of its lower critical solution temperature (LCST) at ~ 32 ^{o}C [7-11]. For a single PNIPAAm chains, it adopts a random coil conformation in aqueous solution below the LCST. Upon heating up to the LCST or higher, the random coil would collapse into a globule owing to dehydration. In the present case, each PNIPAAm chain was grafted onto a bulky and hydrophobic MOSS backbone and only possessed one free end. It is of interest to examine the effect of the macrocyclic brush architecture on the LCST behavior of PNIPAAm chains. The thermoresponsive behavior was investigated by means of micro-differential scanning calorimetry (Micro-DSC) and UV-Vis spectroscopy, respectively. Shown in Figure 6 are the Micro-DSC curves of the aqueous solutions of the organic-inorganic molecular brushes. In the Micro-DSC curves, plain PNIPAAm displayed a single exothermic transition at 33.3 ^{o}C, attributable to the lower critical solution temperature (LCST) of this polymer. The exothermic transition stemmed from the coil-to-globule transition of the hydrated PNIPAAm chains. Notably, all the PNIPAAm@MOSS samples displayed the similar exothermic transitions. These exothermic peaks were asymmetrical with steep leading regions before approaching the minima. It is noted that the LCSTs of all the organic-inorganic molecular brushes were significantly lower than that of plain PNIPAAm. The decreased LCSTs are attributable to the inclusion of the hydrophobic backbones (*viz.* MOSS), which reduced the affinity of PNIPAAm chains with water molecules. It is seen that the LCSTs of the hybrid molecular brushes decreased with decreasing the lengths of PNIPAAm chains. Also shown in Figure 6 is the plot of the endothermic enthalpy (ΔH_{LCST}) as a function of mass percentage of MOSS (See the inset). Assuming that the value of LCST enthalpy (denoted ΔH_{LCST}) is proportional to the quantity of the PNIPAAm chains which underwent the coil-to-globule transition, a

straight line should be drawn according to the mass fraction of PNIPAAm chains if the LCST behavior of PNIPAAm chains were not affected by MOSS. However, the experimental ΔH_{LCST} was negatively deviated from this straight line. This observation suggested that the fractions of the PNIPAAm chains which can undergo the coil-to-globule transition in the organic-inorganic molecular brushes were significantly smaller than plain PNIPAAm. It is proposed that owing to the restriction of MOSS those PNIPAAm segments which were closely connected to MOSS macrocycles were unable to undergo the coil-to-globule transition, *i.e.,* these PNIPAAm segments still remained hydrophilic even while the solutions were heated to above the LCST. This speculation can be confirmed by means of cloud-point analysis and DLS (See *infra*).

The LCST behavior of the organic-inorganic PNIPAAm molecular brushes was further investigated in term of cloud-point analysis by means of UV-Vis spectroscopy. Shown in Figure 7 are the plots of visible light transmittance for the organic-inorganic molecular brushes as functions of temperature. For comparison, the curve of plain PNIPAAm (M_n=12,400 M_w/M_n=1.26) aqueous solution was included. At the low temperature, the optical transmittance of all the aqueous solutions was as high as 97 %. It is noted that the optical transmittance of the PNIPAAm@MOSS suspension was slightly lower than that of plain PNIPAAm. Upon heating the aqueous solutions to the specific temperatures, the optical transmittance was significantly decreased, indicating the occurrence of the coil-to-globule transitions. For plain PNIPAAm, the LCST was measured to be *c.a.* 32 ^{o}C and the transition range of temperature was as narrow as 2 ~ 3 ^{o}C. After the LCST the optical transmittance were decreased to *c.a.* 50 % at 44 ^{o}C. Nonetheless, the PNIPAAm@MOSS suspensions displayed the features quite different from plain PNIPAAm. First, the LCSTs of the PNIPAAm@MOSS samples were much lower than plain PNIPAAm; the LCSTs decreased with decreasing the lengths of PNIPAAm chains in the organic-organic molecular brushes. This observation was in good agreement with the Micro-DSC results. Second, the coil-to-globule transition ranges of the PNIPAAm@MOSS samples were significantly broadened, especially for the sample with the shorter PNIPAAm chains (*e.g.,* PNIPAAm2K@MOSS). The broadened coil-to-globule transition ranges could be associated with the restriction of MOSS on the coil-to-globule transitions of PNIPAAm chains. It is plausible to propose that the

conformational alteration of PNIPAAm chains was hindered by the bulky MOSS backbone while the coil-to-globule transition of PNIPAAm side chains occurred. Third, the optical transmittance of all the organic-inorganic molecular brushes at elevated temperature was significantly higher than the plain PNIPAAm. For instance, the optical transmittance of PNIPAAm10k@MOSS at 44 ^{o}C was still as high as 93 % (See the inset, the optical images of the aqueous solution at 24 and 44 ^{o}C), suggesting that there was considerable portion of the PNIPAAm chain which remained hydrated even at the temperature above the LCSTs. This observation can be accounted for the restriction of MOSS on the coil-to-globule transition of PNIPAAm. This restriction resulted in the failure that the PNIPAAm segments became dehydrated above the LCST. The similar case has been theoretically rationalized by some investigators [45-46] and was found in organic PNIPAAm brushes [47-52].

Self-assembly Behavior in Bulks and Aqueous Solutions

The morphologies of the organic-inorganic molecular brushes in bulks were investigated by means of transmission electron microscopy (TEM). Shown in Figure 8 are the TEM micrographs of PNIPAAm2K@MOSS, PNIPAAm4K@MOSS, PNIPAAm6K@MOSS, PNIPAAm8K@MOSS and PNIPAAm10K@MOSS. Notably, microphase-separated morphologies were exhibited in all the cases. It is seen that he spherical microdomains at the size of 10 ~ 50 nm in diameter were dispersed in a continuous matrix depending on the lengths of PNIPAAm chains. According to the difference in electron density between MOSS and PNIPAAm chains, the spherical microdomains are assignable to MOSS aggregates whereas the continuous matrix to PNIPAAm. Notably, the size of MOSS microdomains decreased with increasing the lengths of PNIPAAm. The formation of the microphase-separated morphologies is attributable to the immiscibility of the inorganic backbone (*viz.* MOSS) with PNIPAAm chains; the spherical MOSS microdomains were formed *via* MOSS-MOSS interactions.

In views of the hydrophobicity of MOSS backbone and the water-solubility of PNIPAAm chains, it is expected that the organic-inorganic molecular brushes would exhibit the self-assembly behavior in aqueous solutions. The self-assembly behavior of the organic-inorganic molecular brushes was investigated by means of

transmission electron microscopy (TEM) and dynamic light scattering (DLS). Shown in Figure 9 are the TEM micrographs of the aqueous solutions after freeze-drying. It is seen that in the aqueous solutions, PNIPAAm2K@MOSS and PNIPAAm4K@MOSS were self-assembled into worm-like and inter-connected nanoobjects (Figures 9A and 9B). With increasing the lengths of PNIPAAm chains, the organic-inorganic molecular brushes were gradually self-assembled into the spherical nanoobjects with the size of 100 ~ 150 nm (See Figures 9C, 9D and 9E). Shown in Figure 10 are the plots of hydrodynamic radius distribution as functions of hydrodynamic radius (R_h) for the aqueous solutions of the PNIPAAm@MOSS samples at 24 and 48 ^oC. Notably, all the organic-inorganic macrocyclic molecular brushes were capable of self-organizing into the nanoobjects in aqueous solution. Apart from PNIPAAm2K@MOSS, the intensity-averaged hydrodynamic radius (R_h) of all other PNIPAAm@MOSS samples displayed unimodal distribution depending on the lengths of PNIPAAm arms at 24 ^oC. Depending on the lenghts of PNIPAAm arms, the values of intensity-averaged hydrodynamic radius (R_h) were measured to be 239, 231, 226, 194 and 162 nm for PNIPAAm2K@MOSS, PNIPAAm4K@MOSS, PNIPAAm6K@MOSS, PNIPAAm8K@MOSS and PNIPAAm10K@MOSS at 24 ^oC, respectively; the R_h values decreased with increasing the length of PNIPAAm arms. It is proposed that the self-assembled nanoobjects are micelle-like aggregates composed of the hydrophobic cores *via* the MOSS-MOSS interactions and the hydrated PNIPAAm coronas. It should be pointed out that for the aqueous solution containing PNIPAAm2K@MOSS, there were the nanoobjects with smaller size (*i.e.,* R_h=32 nm). The bimodal distribution of the hydrodynamic radius could result that the hydrophilicity/hydrophobicity balance was not fully established under the present condition while the percentage of the inorganic hydrophobic component (*viz.* MOSS-MOSS) was too high. The results of DLS further were in good agreement with those of TEM. It is should be pointed out that the sizes of aggregates measured with TEM (Figure 9) were not necessarily identical with the R_h values by means of DLS. The former were obtained in the dry state and are much lower than the latter obtained in solution, which contains the dominant contribution of the solvated coronas (*viz.* PNIPAAm).

Returning to Figure 10, the coil-to-globule transition restriction of MOSS on PNIPAAm chains can be accounted for the hydrodynamic radii at a temperature higher

than the LCSTs (*e.g.,* 48 ^{o}C). At 48 ^{o}C, the R_h values of PNIPAAm10K@MOSS, PNIPAAm8K@MOSS and PNIPAAm6K@MOSS were measured to be 412, 246 and 224 nm, respectively. The increased R_h values are readily interpreted on the basis of the occurrence of the coil-to-globule transition of PNIPAAm chains. With this transition, a portion of PNIPAAm chains became dehydrated. To establish a new hydrophobic/hydrophilic balance even at the elavted temperature, the organic-inorganic molecular brushes were self-organzied into the bigger nanoobjects. For PNIPAAm6K@MOSS, PNIPAAm4K@MOSS and PNIPAAm2K@MOSS, however, the R_h values remained unchanged or even decreased, suggesting that in these systems, a considerable amount of PNIPAAm that remains still hydrated at this temperature. Owing to the presence of these hydrated PNIPAAm chains, the structural arrangement of the original aggregates resulted in the decreased size of the nanoobjects, to meet the new hydrophilic/hydrophobic balance. Notably, although the decreased R_h values were observed for PNIPAAm4K@MOSS and PNIPAAm2K@MOSS at 48 ^{o}C, the distribution of R_h became fairly broad due possibly to the restriction of MOSS on PNIPAAm chains.

CONCLUSIONS

The organic-inorganic molecular brushes composed of macrocyclic oligomeric silsesquioxanes (MOSS) and poly(N-isopropyl acrylamide) (PNIPAAm) chains were synthesized *via* the atom transfer radical polymerization (ATRP) with a 24-membered MOSS macromer bearing twelve 2-chloropropionate moieties. Gel permeation chromatography (GPC) showed that the polymerization of N-isopropyl acrylamide (NIPAAm) mediated by copper (I) chloride and tris(2-(dimethylamino)ethyl)amine (Me_6TREN) was in a living and controlled manner. Transmission electron microscopy (TEM) showed that the organic-inorganic molecular brushes were microphase-separated. The self-assembly of the organic-inorganic molecular brushes in bulks resulted in the formation of the morphology in which the spherical MOSS microdomains with the size of 10 ~ 50 nm in diameter were dispersed into continuous PNIPAAm matrix. All the organic-inorganic molecular brushes can be dispersed in water. The PNIPAAm@MOSS samples were capable of self-organizing into the spherical nanoobjects in aqueous solutions as evidenced by dynamic light scattering

(DLS) and transmission election microscopy (TEM). The size of the nanoobjects was quite dependent on the percentage of MOSS in the organic-inorganic molecular brushes. Both micro-differential scanning calorimetry (Micro-DSC) and ultraviolet-visible spectroscopy showed that the organic-inorganic molecular brushes can exhibit the thermoresponsive properties in aqueous solution as plain PNIPAAm homopolymer. Nonetheless, the MOSS cages in the molecular brushes exerted the significant restriction of coil-to-globule transition of PNIPAAm chains.

ACKNOWLEDGMENT

The financial supports from Natural Science Foundation of China (No. 21274091 and 51133003) were gratefully acknowledged.

REFERENCES

1. Y. C. Wang, L. Tang, Y. Li, J. Wang, *Biomacromolecules*, 2008, **10**, 66.
2. A. W. York, S. E. Kirkland, C. L. McCormick, *Adv. Drug Delivery Rev.,* 2008, **60**, 1018.
3. Y. Hu, Y. Chen, Q. Chen, L. Y. Zhang, X. Q. Jiang, C. Z. Yang, *Polymer*, 2005, **46**, 12703.
4. Z. L. Ding, R. B. Fong, C. J. Long, P. S. Stayton, A. S. Hoffman, *Nature*, 2001**,** **411**, 59.
5. Y. F. Zhang, S. Z. Luo, S. Y. Liu, *Macromolecules*, 2005, **38**, 9813.
6. P. De, S. R. Gondi, D. Roy, B. S. Sumerlin, *Macromolecules*, 2009, **42**, 5614.
7. M. Heskins, J. E. Guillet, *J. Macromol. Sci., A: Chem.*, 1968, **2**, 441.
8. P. Kujawa, F. Tanaka, F. M. Winnik, *Macromolecules,* 2006, **39**, 3048.
9. H. G. Schild, *Prog. Polym. Sci.*, 1992, **17**, 163.
10. C. Wu, *Macromolecules*, 1997, **30**, 574.
11. P. Kujawa, F. M. Winnik, *Macromolecules*, 2001, **34**, 4130.
12. Y. Hirokawa, T. Tanaka, *J. Chem. Phys.*, 1984, **81**, 6379.
13. E. S. Matsuo, T. Tanaka, *J. Chem. Phys.,* 1988, **89**, 1695.

14. A. Suzuki, T. Tanaka, *Nature*, 1990, **346***,* 345.
15. K. Otake, H. Inomata, M. Konno, S. Saito, *Macromolecules*, 1990, **23***,* 283.
16. H. Inomata, S. Goto, K. Otake, S. Saito, *Langmuir*, 1992, **8***,* 687.
17. M. Shibayama, M. Morimoto, S. Nomura, *Macromolecules*, 1994, **27***,* 5060.
18. L. Liang, P. C. Rieke, J. Liu, G. E. Fryxell, J. S. Young, M. H. Engelhard, K. L. Alford, *Langmuir*, 2000, **16***,* 8016.
19. J. Shan, J. Chen, M. Nuopponen, H. Tenhu, *Langmuir*, 2004, **20***,* 4671.
20. M. Nuopponen, J. Ojala, H. Tenhu, *Polymer*, 2004, **45***,* 3643.
21. X. Zhou, X. Ye, G. Zhang, *J. Phys. Chem. B.*, 2007**, 111***,* 5111.
22. J. Mu, S. Zheng, *J. Colloid & Interface Sci.*, 2007, **307***,* 377.
23. K. Zeng, Y. Fang, S. Zheng, *J. Polym. Sci., Part B: Polym. Phys.*, 2009**, 47***,* 504.
24. W. Zhang, L. Liu, X. Zhuang, X. Li, J. Bai, Y. Chen, *J. Polym. Sci., Part A: Polym. Chem.*, 2008**, 46**, 7049.
25. Y. Zheng, L. Wang, S. Zheng, *Eur. Polym. J.*, 2012, **48**, 945.
26. L. Wang, K. Zeng, S. Zheng, *ACS Appl. Mater. & Interface*, 2011**, 3***,* 898.
27. S. W. Kuo, J. L. Hong, Y. C. Huang, J. K. Chen, S. K. Fan, F. H. Ko, C. W. Chu, F. C. Chang, *J. Nanomater.*, 2012**,** Art. ID: 749732, doi:10.1155/2012/749732;
28. Y. Bai, J. Wei, L. Yang, C. He, X. Lu, *Colloid Polym. Sci.*, 2012**, 290***,* 507.
29. G. Li, L. Wang, H. Ni, C. U. Pittman, *J. Inorg. Organomet. Polym.*, 2001, **11**, 123.
30. O. I. Shchegolikhina, V. A. Igonin, Y. A. Molodtsova, Y. A. Pozdnyakova, *J Organomet Chem.*, 1998, **562**, 141.
31. A. A. Zhdanov, T. V. Strelkova, *J. Organomet. Chem.*, 1998, **562**, 141.
32. N. V. Sergienko, E. S. Trankina, V. I. Pavlov, A. A. Zhdanov, K. A. Lyssenko, M. Y. Antipin, *Russ. Chem. Bull. Int. Ed.*, 2004, **53**, 351.
33. Y. A. Molodtsova, Y. A. Pozdnyakova, K. A. Lyssenko, I. V. Blagodatskikh, D. E. Katsoulis, O. I. Shchegolikhina, *J. Organomet. Chem.*, 1998, **571**, 31.
34. O. I. Shchegolikhina, Y. A. Pozdnyakova, S. D. Molodtsova, B.Korkin, *Organometallics*, 2000, **19**, 1077.
35. O. I. Shchegolikhina, Y. A. Pozdnyakova, Y. A. Molodtsova, S. D. Korkin, S. S.

Bukalov, L. A. Leites, K. A. Lyssenko, A. S. Peregudov, N. Auner, D. E. Katsoulis, *Inorg. Chem.*, 2002, **41**, 6892.

36. Y. A. Pozdnyakova, K. A. Lyssenko, I. V. Blagodatskikh, N. Auner, D. E. Katsoulis, O. I. Shchegolikhina, *Eur. J. Inorg. Chem.*, 2004, **2004**, 1253.
37. O. I. Shchegolikhina, Y. A. Pozdnyakova, M. Y. Antipin, D. E. Katsoulis, N. Auner, B. Herrschaft, *Organometallics*, 2000, **19**, 1077.
38. J. Han, S. Zheng, *Macromolecules*, 2008, **41**, 4561.
39. J. Han, S. Zheng, *J. Polym. Sci., Part A: Polym. Chem.*, 2009, **47**, 6894.
40. J. Han, L. Zhu, S. Zheng, *Eur. Polym. J.*, 2012, **48**, 730.
41. L. Zhu, C. Zhang, J. Han, S. Zheng, *Soft Matter*, 2012, **8**, 7062.
42. J. S. Wang, K. Matyjaszewski, *J. Am. Chem. Soc.*, 1995, **117**, 5614.
43. Y. A. Molodtsova, K. A. Lyssenko, I. V. Blagodatskikh, E. V. Matukhina, A. S. Peregudov, M. I. Buzin, V. G. Vasil'ev, D. E. Katsoulis, O. I. Shchegolikhina, *J. Organomet. Chem.*, 2008, **693**, 1797.
44. Y. A. Molodtsova, Y. A. Pozdnyakova, I. V. Blagodatskikh, A. S. Peregudov, O. I. Shchegolikhina, *Russ. Chem. Bull. Int. Ed.*, 2003, **52**, 2722.
45. E. B. Zhulina, O. V. Borisov, V. A. Pryamitsyn, T. M. Birshtein, *Macromolecules*, 1991, **24***,* 140.
46. G. S. Grest, M. Murat, In *Monte Carlo and Molecular Dynamics Simulations in Polymer Science* (K. Binder, Ed.), Clarendon: Oxford, 1994;
47. G. E. Yakubov, B. Loppinet,; H. Zhang, J. Ru¨he, R. Sigel, G. Fytas, *Phys. Rev Lett.*, 2004, **92***,* 115501.
48. A. Domack, S. Prucker, J. Ruhe, D. Johannsmann, *Phys. Rev. E*, 1997, **56***,* 680.
49. A. Karim, S. K. Satija, J. F. Douglas, J. F. Ankner, L. J. Fetters, *Phys. Rev. Lett.*, 1994, **73***,* 3407.
50. S. Balamurugan, S. Mendez, S. S. Balamurugan, M. J. II. O' Brien, G. P. Lopez, *Langmuir* , 2003, **19***,* 2545.
51. H. Yim, M. S. Kent, S. Mendez, S. S. Balamurugan, S. Balamurugan, G. P. Lopez, S. Satija, *Macromolecules*, 2004, **37***,* 1994.
52. P. W. Zhu, D. H. Napper, *Langmuir*, 1996, **12**, 5992.

SCHEMES

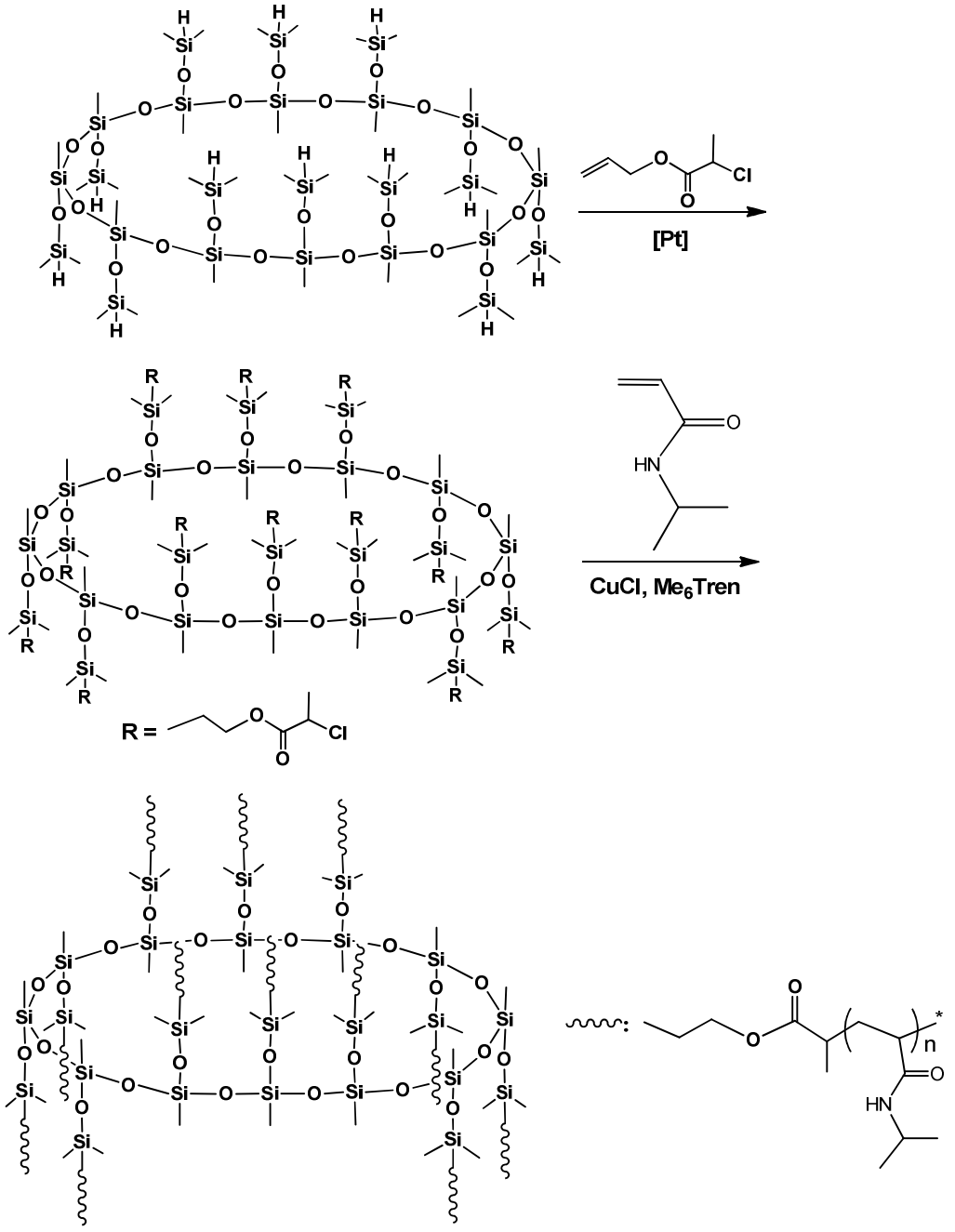

Scheme 1 Synthesis of organic-inorganic molecular brushes composed of MOSS and PNIPAAm

Table 1 Results of polymerization for the preparation of organic-inorganic molecular brushes composed of MOSS and PNIPAAm

Sample	L_{arm}(PNIPAAm)	M_n(Da)[a]	M_w/M_n	M_n(Da)[b]
PNIPAAm10K@MOSS	10,100	124,800	1.30	126,200
PNIPAAm8K@MOSS	7,700	95,600	1.41	113,560
PNIPAAm6K@MOSS	5,600	70,200	1.43	72,800
PNIPAAm4K@MOSS	4,300	54,900	1.45	66,720
PNIPAAm2K@MOSS	2,700	36,200	1.46	42,460
Macroinitiator	-	3,400	1.12	-

a: The values measured by means of gel permeation chromatography (GPC);

b: The values estimated according to thermogravimetric analysis (TGA)

FIGURE CAPTIONS

Figure 1. ^{29}Si NMR spectrum of dodecamethyldodeca(dimethylhydro) cyclododecasilsesquioxane (**1**);

Figure 2. MALDI-TOF mass spectrum of dodecamethyldodeca(dimethylhydro) cyclododecasilsesquioxane (**1**);

Figure 3. ^{1}H NMR spectra of dodecamethyldodeca(dimethylhydro) cyclododecasilsesquioxane (**1**), MOSS macromolecular initiator (**3**) and PNIPAAm2K@MOSS;

Figure 4. GPC profiles of the organic-inorganic macrocyclic molecular brushes;

Figure 5. Plots of number-average molecular weights and polydispersity indices as functions of the molar ratio of NIPAAm to the MOSS macromolecular Initiator (**3**);

Figure 6. Micro-DSC curves of the aqueous solutions of plain PNIPAAm (M_n=12,400 with M_w/M_n=1.26) and the organic-inorganic macrocyclic molecular brushes;

Figure 7. Plots of light transmittance (λ = 550 nm) as functions of temperature for the aqueous solution (0.2g/L) of plain PNIPAAm and PNIPAAm@MOSS samples at the heating rate of 0.2 ^{o}C/min;

Figure 8. TEM micrographs of the organic-inorganic macrocyclic molecular brushes in bulks: A) PNIPAAm10K@MOSS, B) PNIPAAm8K@MOSS, C) PNIPAAm6K@MOSS, D) PNIPAAm4K@MOSS and E) PNIPAAm2K@MOSS;

Figure 9. TEM micrographs of the organic-inorganic macrocyclic molecular brushes in the aqueous solutions at 0.2 g/L: A) PNIPAAm2K@MOSS, B) PNIPAAm4K@MOSS, C) PNIPAAm6K@MOSS, D) PNIPAAm8K@MOSS and E) PNIPAAm10K@MOSS;

Figure 10. Hydrodynamic radius (R_h) of PNIPAAm@MOSS samples in the aqueous solutions (0.2 g/L) at 24 (solid lines) and 48 ^{o}C (dashed lines)

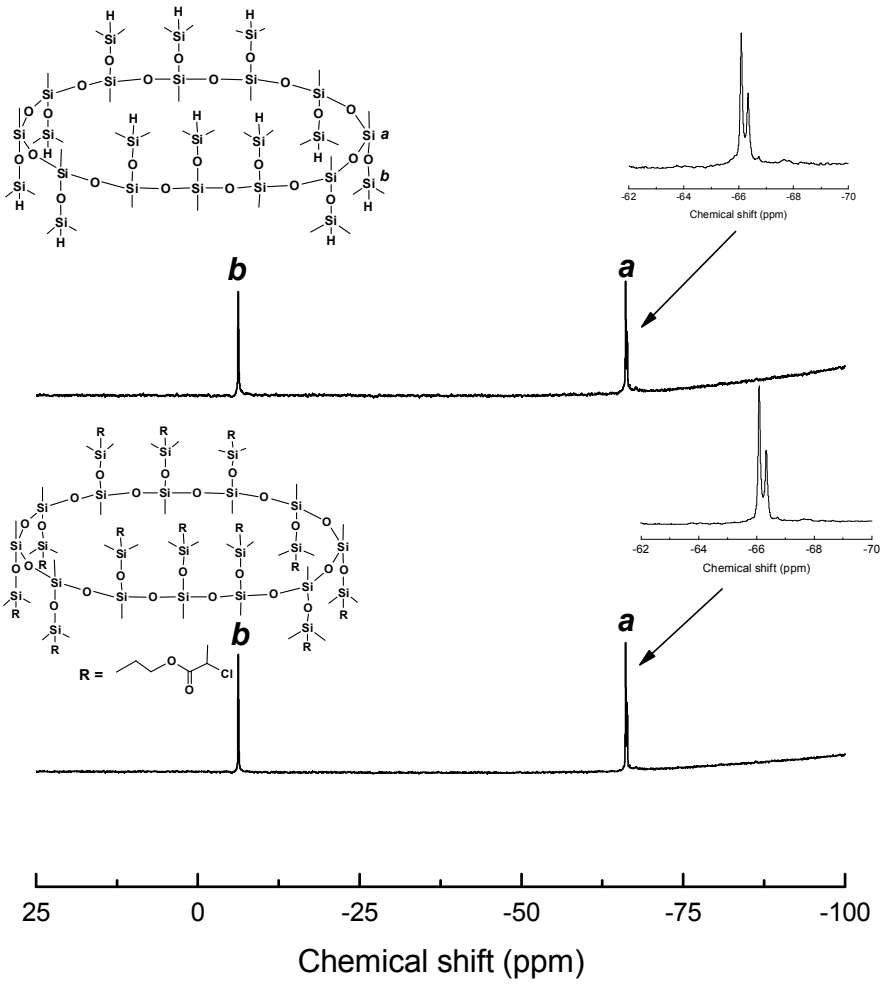

Figure 1

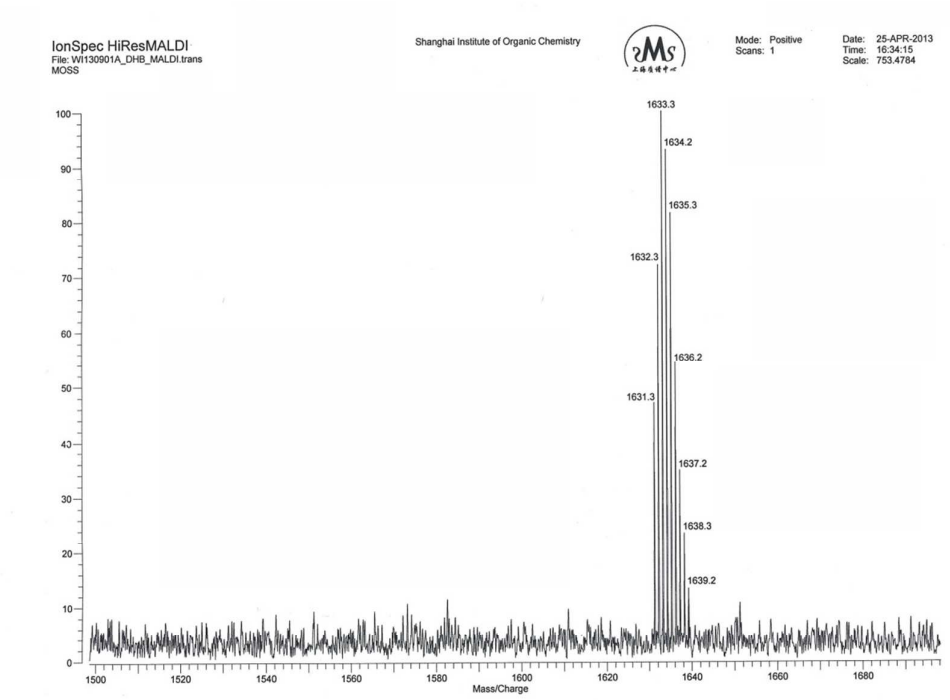

Figure 2

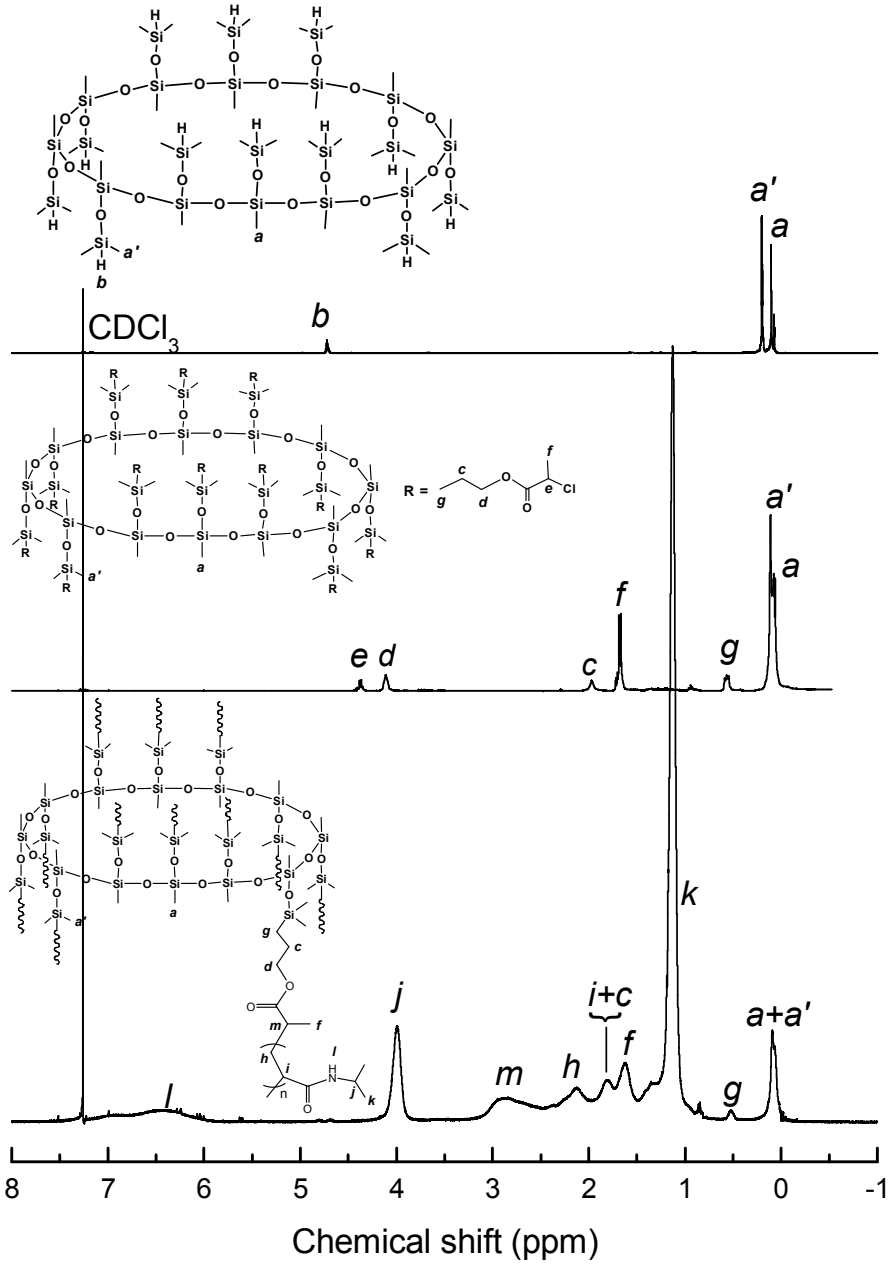

Figure 3

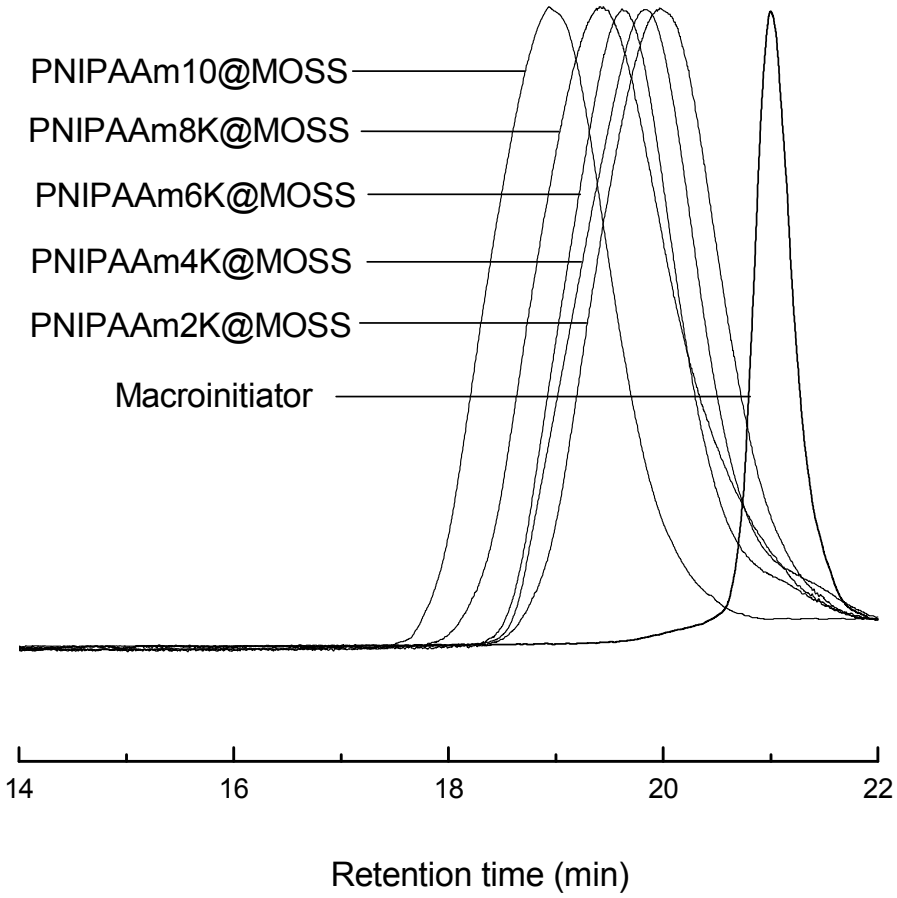

Figure 4

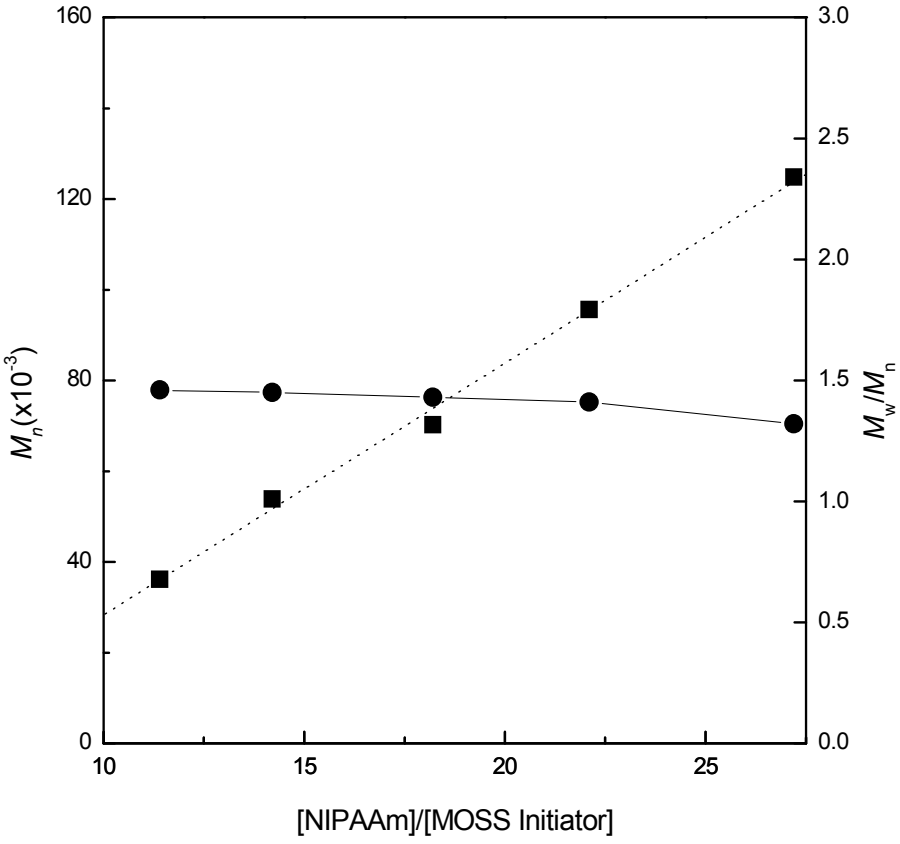

Figure 5

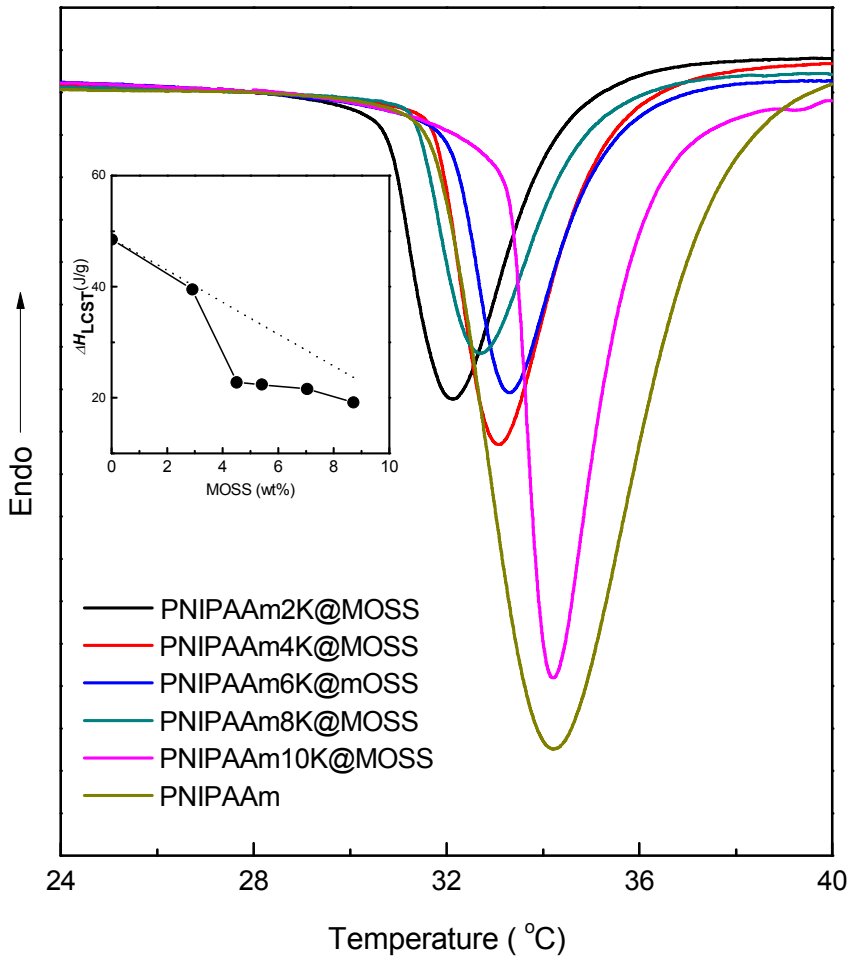

Figure 6

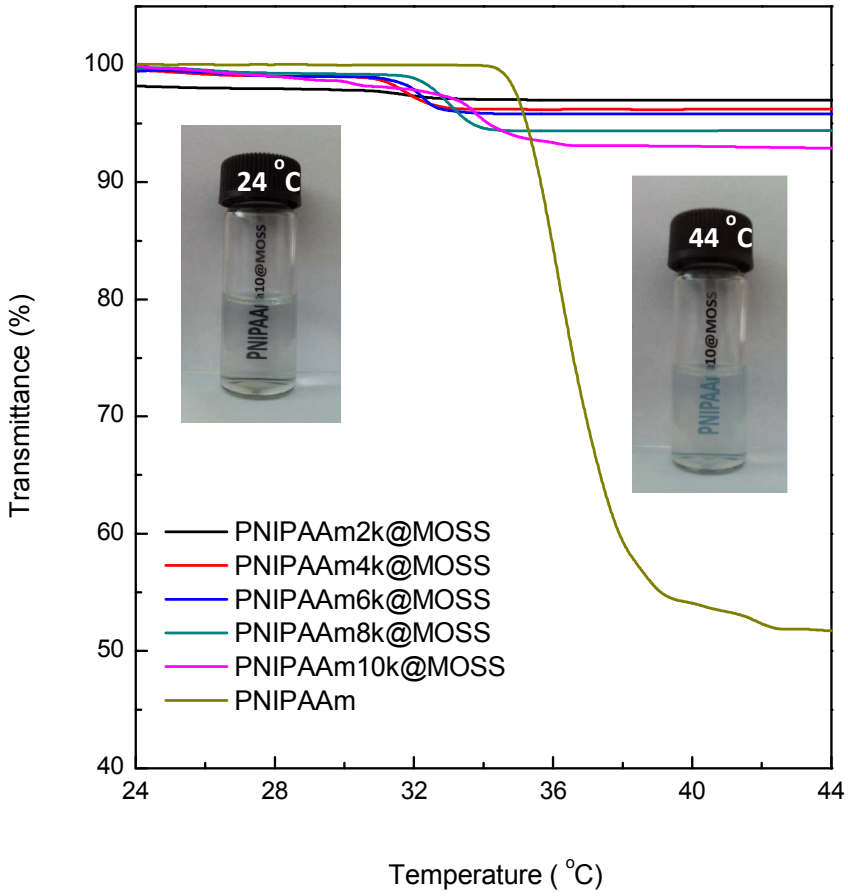

Figure 7

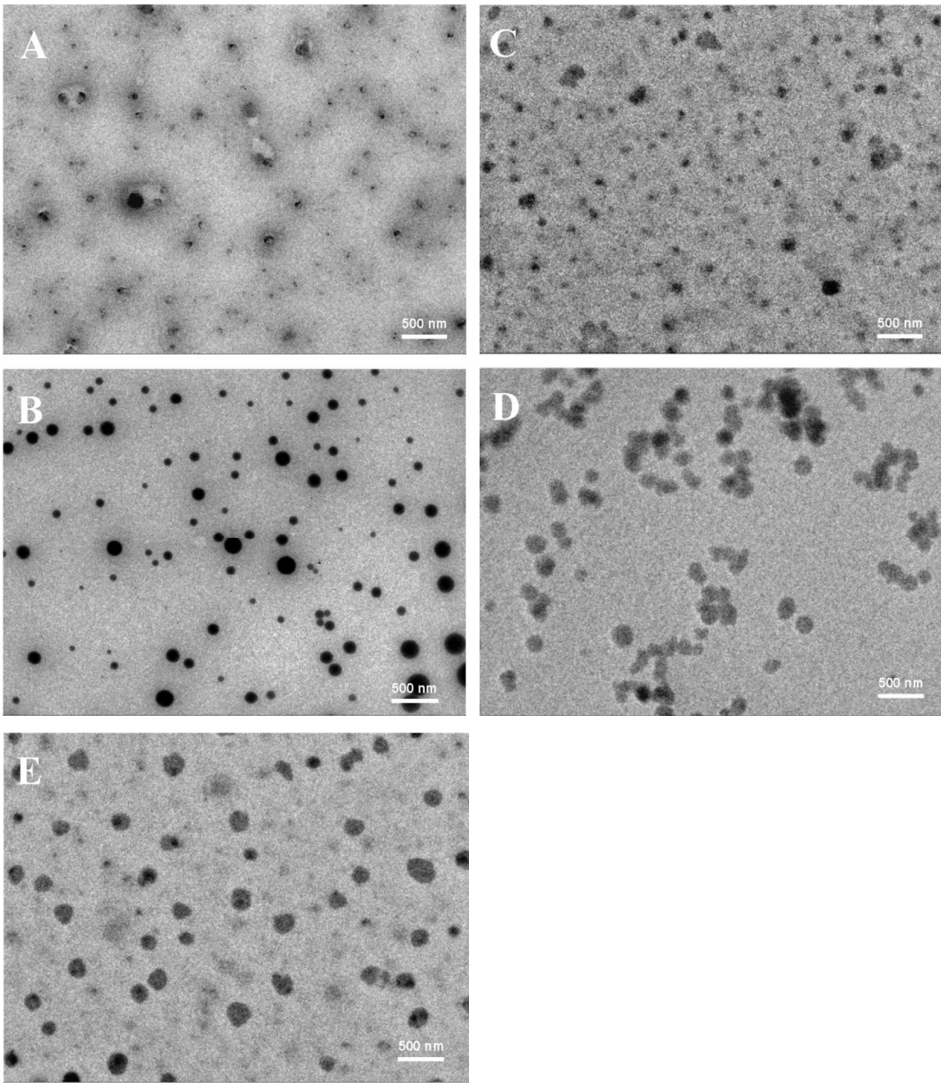

Figure 8

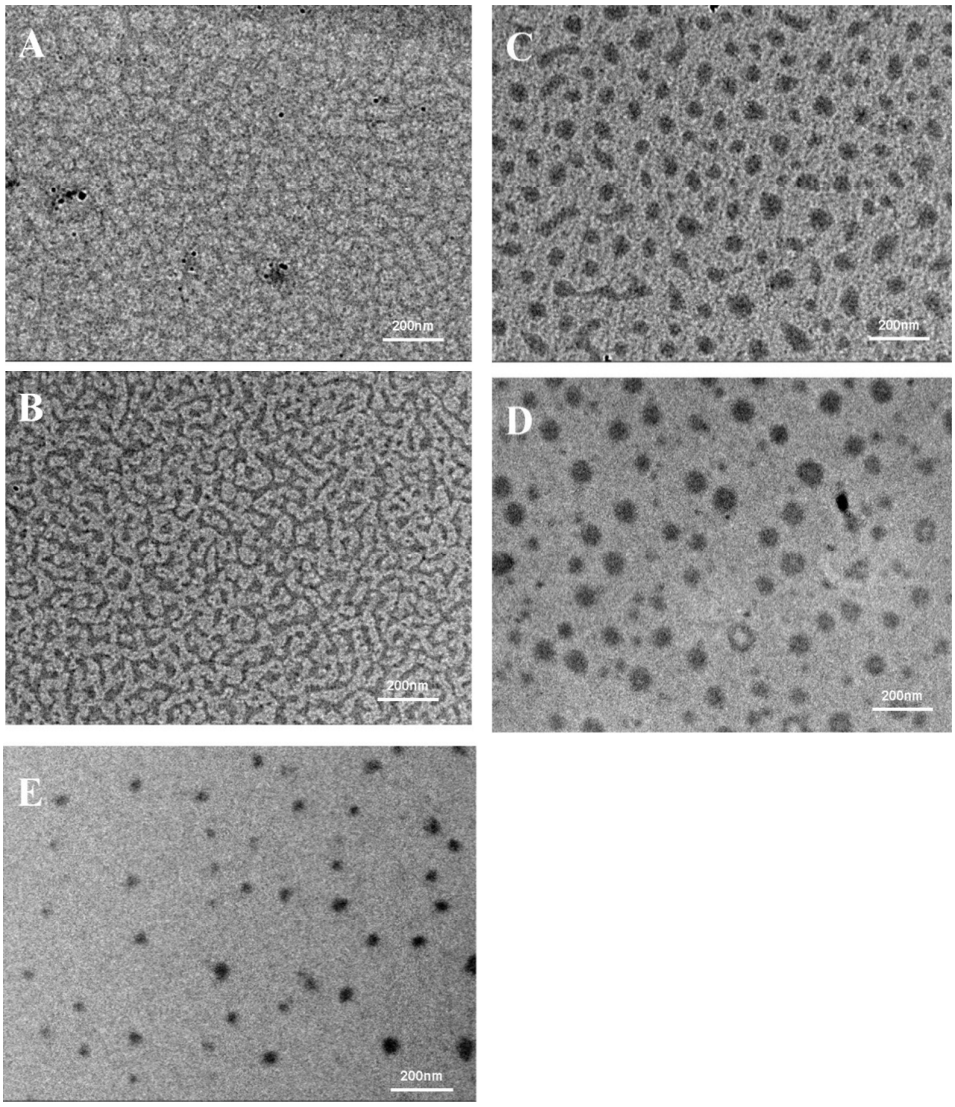

Figure 9

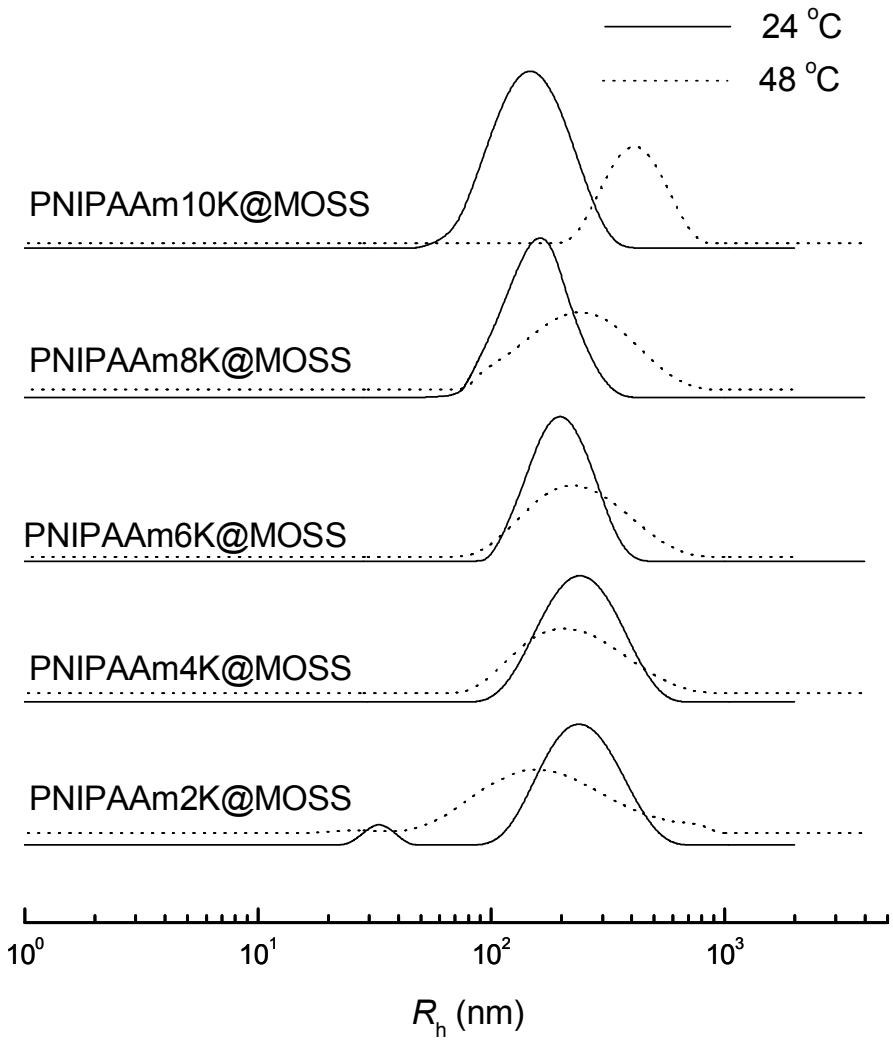

Figure 10